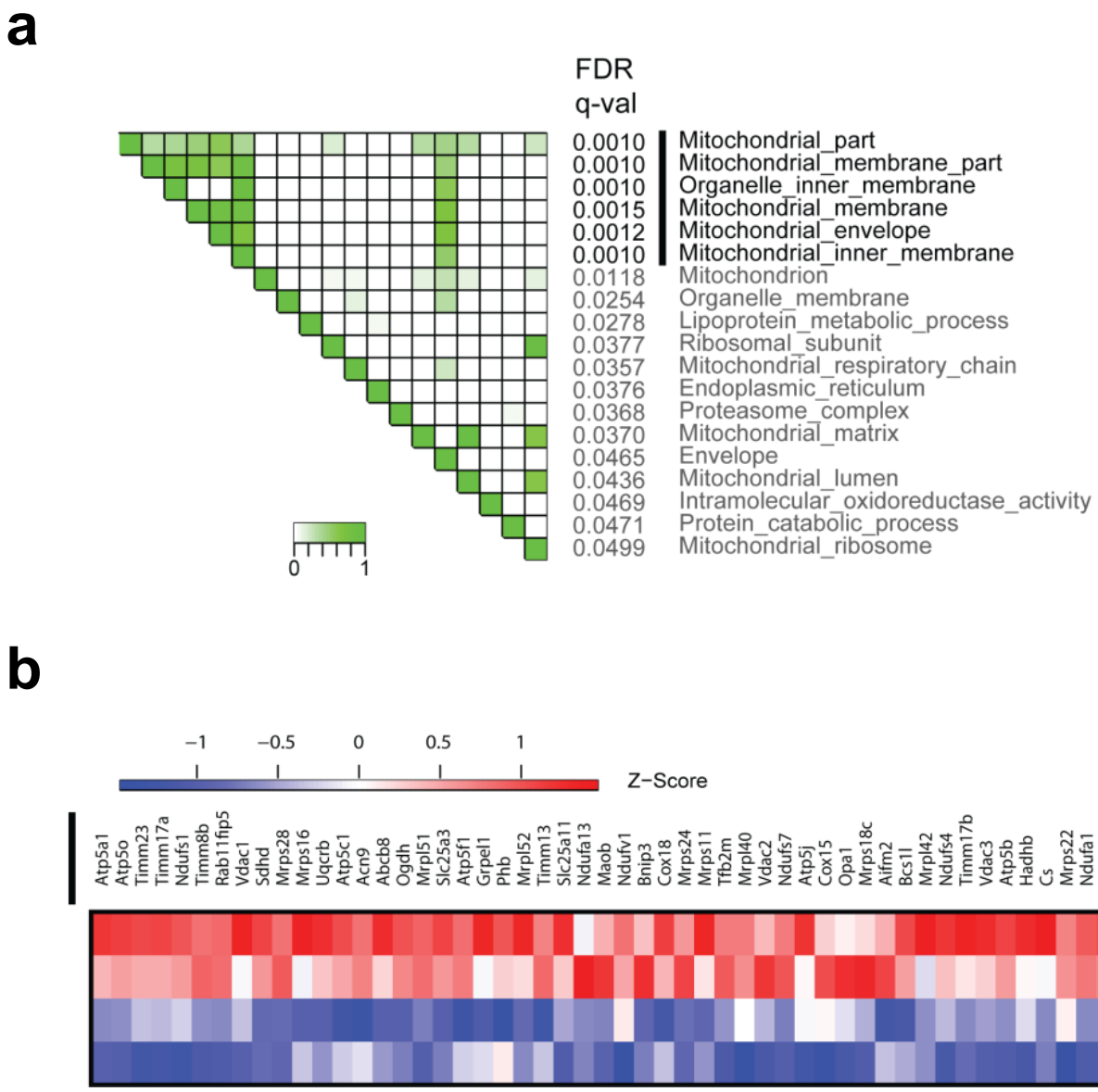


**Supplementary Figure 1. Gene set enrichment analyses.** **(a)** GO gene sets (MSigDB v3. c5) enriched in *KRas;Atg5*$^{fl/+}$ as compared to *KRas;Atg5*$^{fl/fl}$ tumors using gene set enrichment analysis (GSEA) with a false discovery rate (FDR) cut-off of 5%. The set-to-set diagram was created via GSEA leading edge analysis and indicates overlap between the significantly enriched gene-sets. **(b)** Heatmap of the most significantly enriched genes (leading edge genes) from (a) with a FDR below 0.01. Z-scores are indicated.

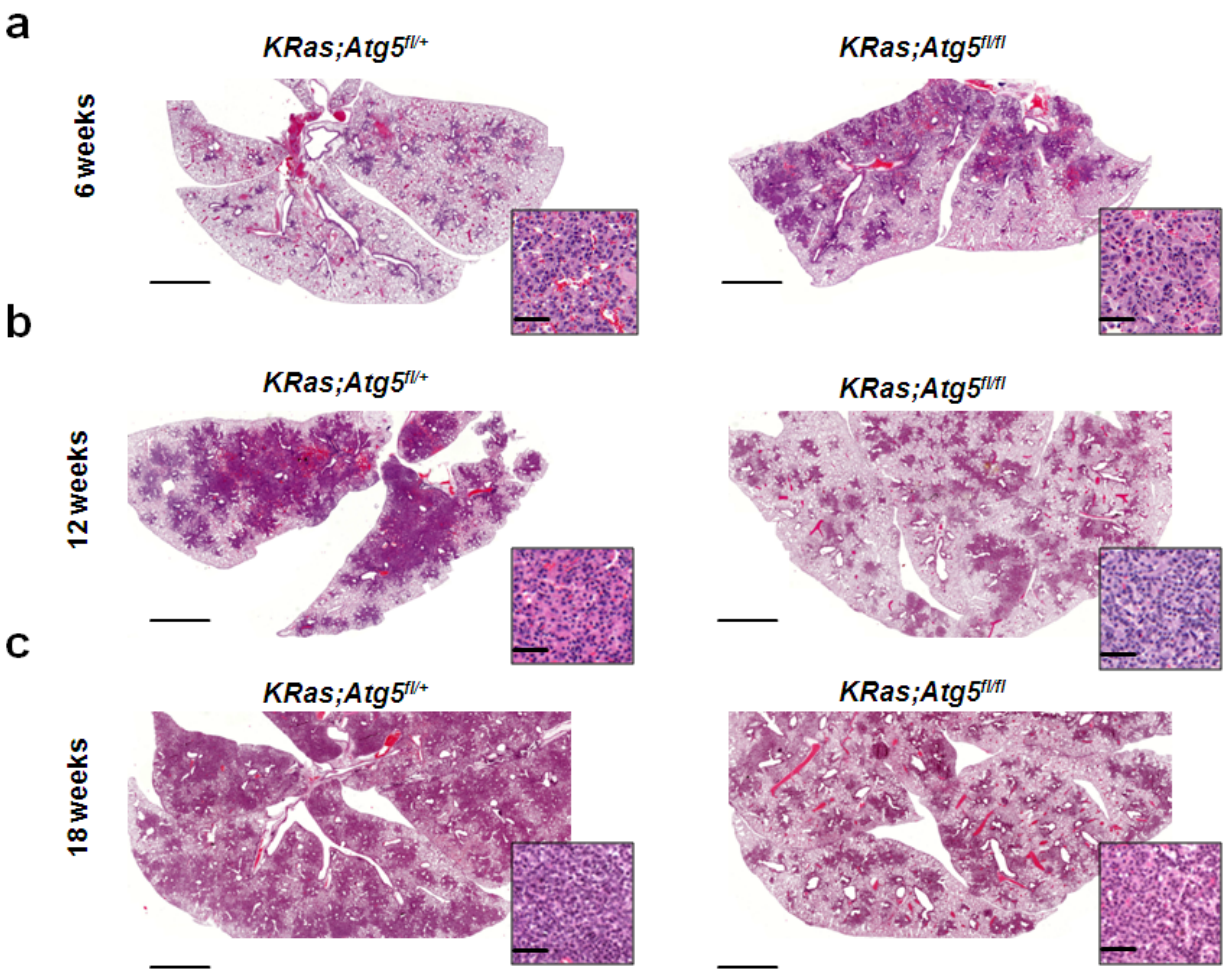


**Supplementary Figure 2. Histology of *Atg5*-deficient KRas$^{G12D}$-driven lung tumors.** **(a-c)** Histological lung sections of *KRas;Atg5*$^{fl/+}$ and *KRas;Atg5*$^{fl/fl}$ littermate mice **(a)** 6 wks, **(b)** 12 wks and **(c)** 18 wks after AdCre inhalation. Representative lung images are shown for each genotype at the indicated time points. Insets show typical lung lesions. Scale bars, 2mm for whole lung section; 50 µm for insets.

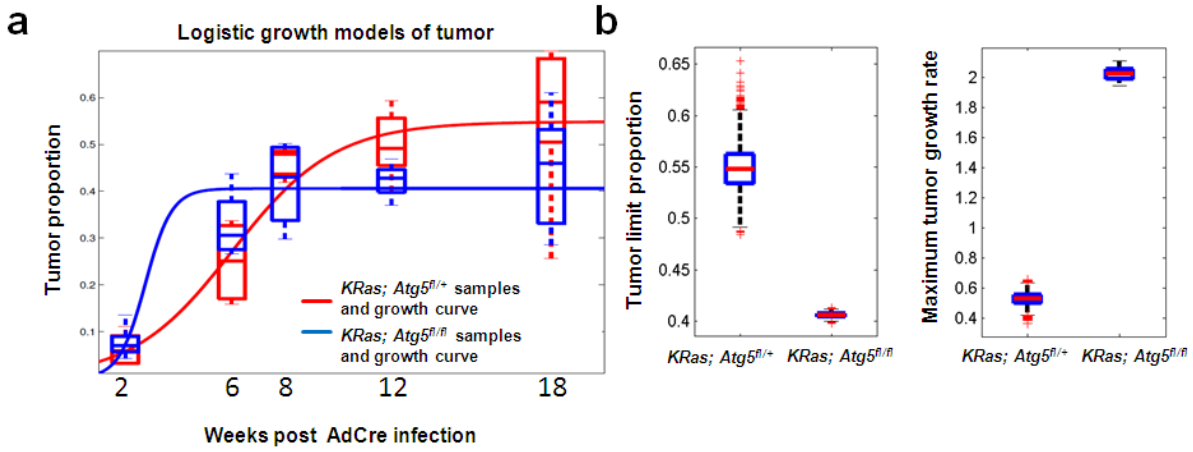


**Supplementary Figure S3. Requirement for Atg5 in KRas$^{G12D}$-driven tumor progression.** **(a)** Logistic growth models, $\alpha(t)=\alpha_\infty 1/(1+$of $1/(1+\exp(\beta-rt)$,of lung tumor proportions, $\alpha(t)$, in lungs of *KRas;Atg5*$^{fl/+}$ and *KRas;Atg5*$^{fl/fl}$ littermate mice. Mean tumor-to-lung area ratios are indicated for individual *KRas;Atg5*$^{fl/+}$ (red) and *KRas;Atg5*$^{fl/fl}$ (blue) mice at the indicated time points following AdCre inhalations. Logistic tumor growth curves were inferred for *KRas;Atg5*$^{fl/+}$ (red line) and *KRas;Atg5*$^{fl/fl}$ (blue line) mice by applying a Bayesian Markov Chain Monte Carlo approach. **(b)** Box blots showing the Bayesian posterior parameter distributions of limit proportions, $\alpha_\infty$, and maximum growth rates, *r*, of lung tumors in *KRas;Atg5*$^{fl/+}$ and *KRas;Atg5*$^{fl/fl}$ littermate mice. The limit proportion of tumor cells for the *KRas;Atg5*$^{fl/fl}$ mice is around 40% and thus significantly smaller than the 55% proportion of tumor cells reached in *KRas;Atg5*$^{fl/+}$ controls. At the same time we also find that *KRas;Atg5*$^{fl/+}$ tumors show a significantly slower maximum growth rate, which explains why they reach the stationarity phase later than *KRas;Atg5*$^{fl/fl}$ lung tumors. The central horizontal line of each box represents the median. The edges of the boxes are the 25th and 75th percentiles. The whiskers extend to the most extreme data points not considered outliers. Outliers are plotted individually. n=at least 4 mice per genotype.

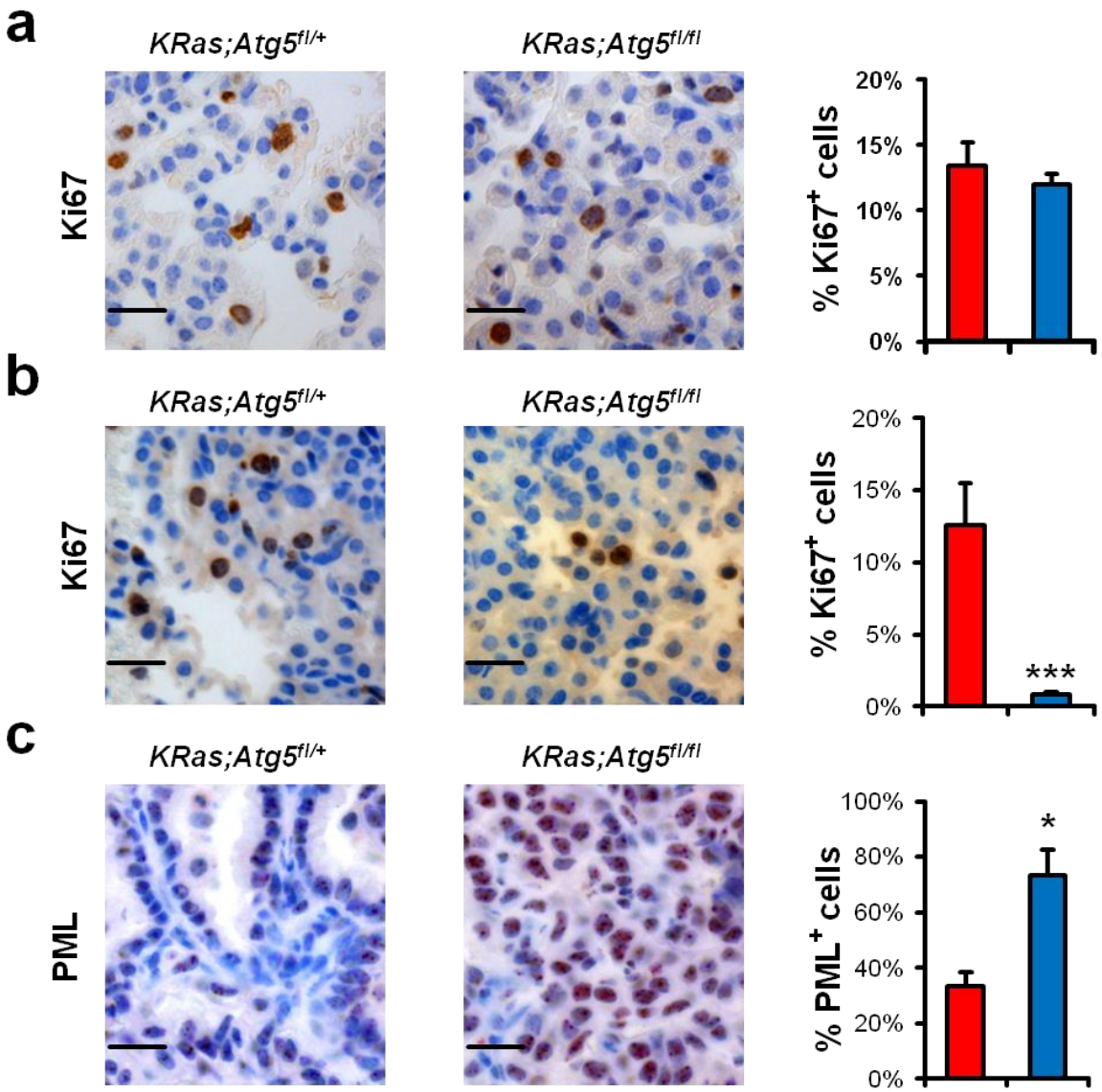


**Supplementary Figure 4. Impaired proliferation and enhanced sensescence of *Atg5* mutant lung tumor cells.** **(a)** Representative immunohistochemisty and quantitative assessment of the proliferation marker Ki67 in lung tumors from *KRas;Atg5*$^{fl/+}$ and *KRas;Atg5*$^{fl/fl}$ littermates 6 wks after AdCre inhalation. Data are shown as mean percentages (±SEM) of positive cells per total tumor cell numbers. Of note, only cells inside the tumors were counted. At least 6 mice per genotype and time point were analyzed. Scale bars, 50μm. **(b, c)** Representative immunohistochemisty and quantitative assessment of **(b)** the proliferation marker Ki67 and **(c)** the senescence marker PML in lung tumors from *KRas;Atg5*$^{fl/+}$ and *KRas;Atg5*$^{fl/fl}$ littermates 18 wks after AdCre inhalation. Sections were scored independently in a double-blinded fashion. Data are shown as mean percentages (±SEM) of positive cells per total cell numbers. Only cells inside the tumors were counted. At least 6 mice per genotype and time point were analyzed. 50μm. * $P < 0.05$, *** $P < 0.001$ (Chi-square test of a generalised linear model with logit link assessing the genotype effect).

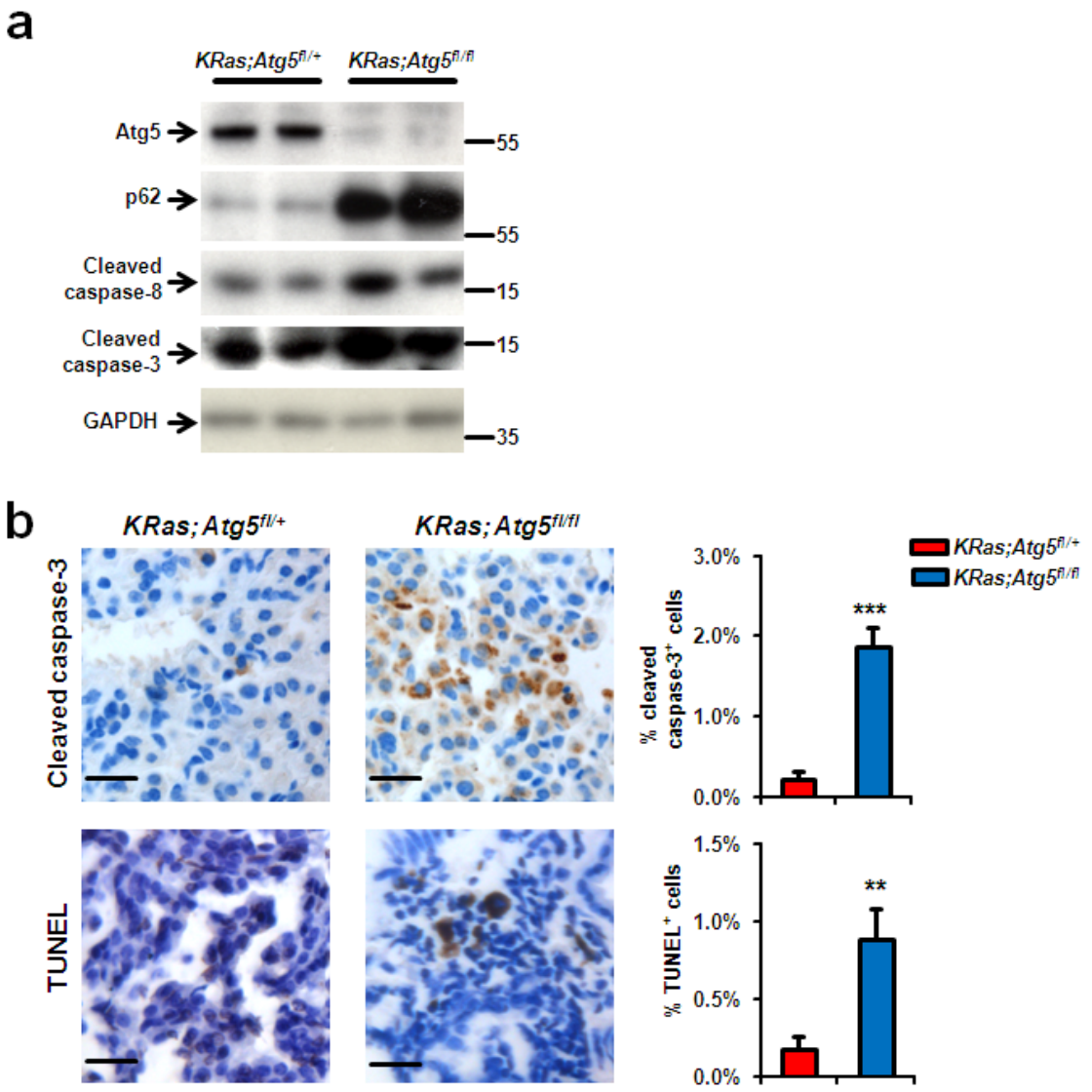


**Supplementary Figure 5. Enhanced cell death of *Atg5* mutant lung tumor cells.** **(a)** Western blot analysis of Atg5, p62, cleaved caspase3, and cleaved caspase8 in tumor tissues 18 wks after AdCre inhalation. Data from two different *KRas;Atg5*$^{fl/+}$ and *KRas;Atg5*$^{fl/fl}$ mice are shown. GAPDH is shown as a loading control. **(b)** Representative immunohistochemisty and quantitative assessment of cleaved caspase3 and Tunel-positive cells in lung tumors from *KRas;Atg5*$^{fl/+}$ and *KRas;Atg5*$^{fl/fl}$ littermates 18 wks after AdCre inhalation. Sections were scored independently in a double-blinded fashion. Data are shown as mean percentages (±SEM) of positive cells per total cell numbers. Only cells within tumors were counted. At least 6 mice per genotype and time point were analyzed. Size bars, 50µm. ** $P < 0.01$; *** $P < 0.001$ (Chi-square tests of a generalised linear model with logit link assessing the genotype effect).

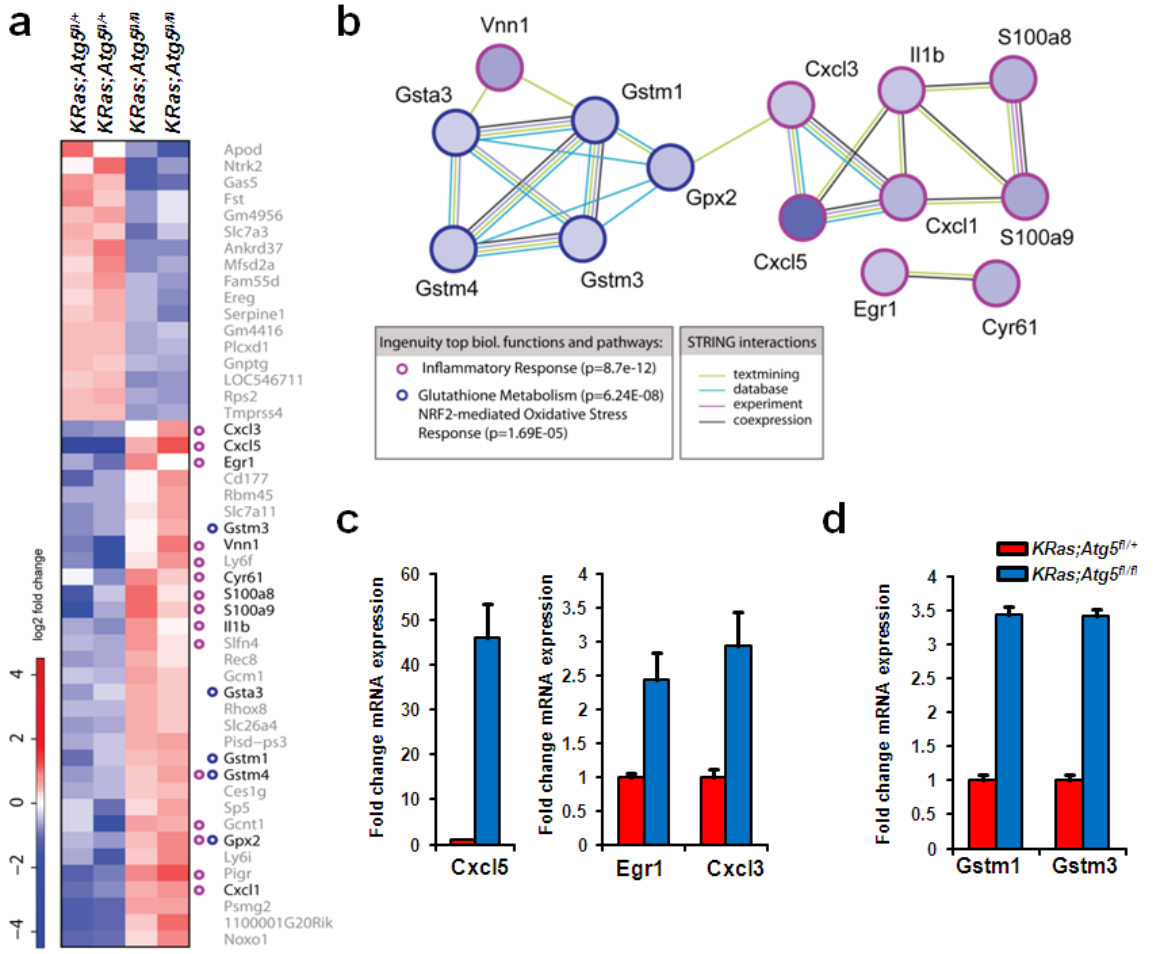


**Supplementary Figure 6. Gene expression profiling and network mapping. (a)** Heatmap visualization of genes showing a higher than twofold difference in expression between *KRas;Atg5*$^{fl/+}$ and *KRas;Atg5*$^{fl/fl}$ tumors (false discovery rate (FDR); $P < 0.05$). Functional classification for these differentially expressed transcripts was performed using Ingenuity pathway Analysis (IPA) and indicates significant enrichment of the categories "Inflammatory Response" (P=8.7E-12), "Glutathione Metabolism" (P=6.24E-08), and "NRF2-mediated Oxidative Stress Response" (P=1.69E-05). Genes assigned to these processes are highlighted using purple and blue circles. **(b)** An interaction network generated using STRING 9.0 shows known and predicted links of proteins within the enriched categories "Inflammatory Response" and "Glutathione Metabolism/NOS" (gene names are also highlighted in the heatmap). **(c,d)** qPCR analyses to confirm deregulated mRNA expression of the **(c)** inflammatory genes Cxcl5, Egr1, and Cxcl3, and **(d)** the oxidative stress genes Gstm1 and Gstm2. Data are shown as mean relative upregulation (±SEM) of mRNA expression in *KRas;Atg5*$^{fl/fl}$ tumors as compared to tumors from *KRas;Atg5*$^{fl/+}$ mice (set to 1). Values were normalized to β-actin mRNA expression. Three different tumors from 3 individual mice/per group were analysed.

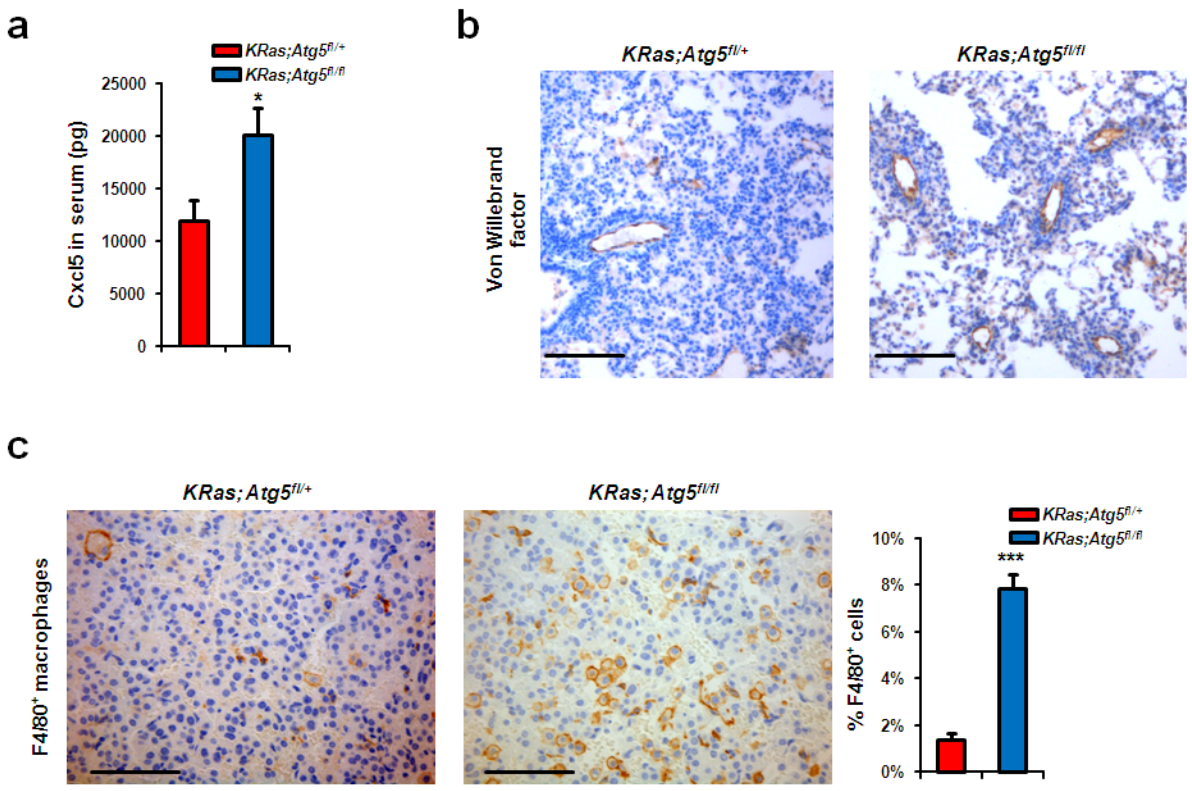


**Supplementary Figure 7. Blood vessel formation and macrophage infiltration in lung tumors.** **(a)** ELISA analysis of Cxcl5 in sera of lung tumor bearing *KRas;Atg5*$^{fl/+}$ and *KRas;Atg5*$^{fl/fl}$ mice 18 wks after tumor induction. Data are shown as mean percentages (± SEM). n = 6 per group. * $P < 0.05$ (Chi-square tests of a generalised linear model with log link assessing the genotype effect). **(b)** Representative immunohistochemistry of Von Willebrand Factor positive blood vessels (arrows) in lung tumors from *KRas;Atg5*$^{fl/+}$ and *KRas;Atg5*$^{fl/fl}$ littermates 18 wks after AdCre inhalation. Size bars, 50µm. **(c)** Representative immunohistochemisty and quantitative assessment of F4/80 positive macrophages in lung tumors from *KRas;Atg5*$^{fl/+}$ and *KRas;Atg5*$^{fl/fl}$ littermates 18 wks after AdCre inhalation. Sections were scored independently in a double-blinded fashion. Data are shown as mean percentages (±SEM) of positive cells per total cell numbers. Only cells within tumors were counted. Six mice were analyzed for each genotype. Size bars, 50µm. *** $P < 0.001$ (Chi-square tests of a generalised linear model with logit link assessing the genotype effect).

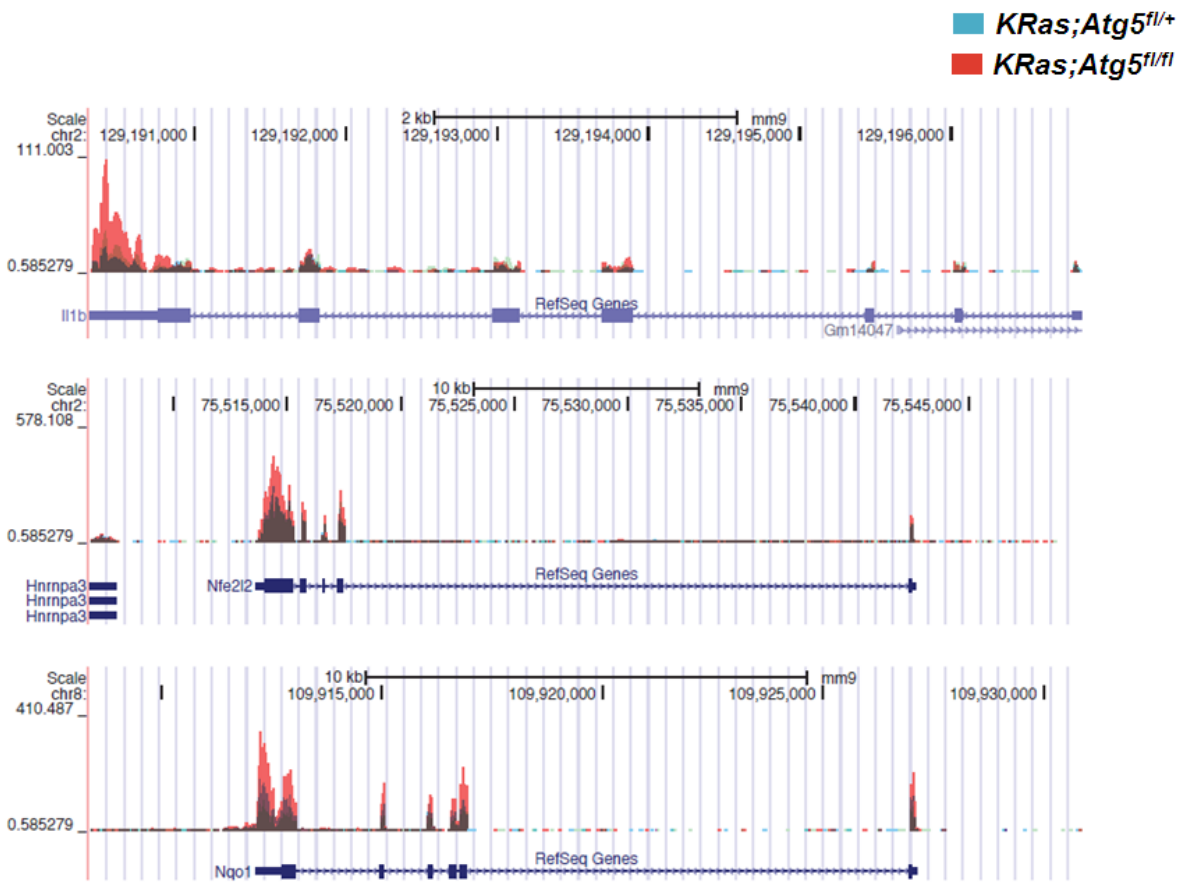


**Supplementary Figure 8. RNAseq data for genes involved in inflammation and oxidative stress responses.** RNA-seq fragment coverage is shown as UCSC multi-experiment overlap track for the inflammatory gene Il1β (upper), Nrf2(middle) and Nqo1(lower), both key genes in the oxidative stress response. polyA-mRNA of *KRas;Atg5*$^{fl/+}$ and *KRas;Atg5*$^{fl/fl}$ pneumocytes after 96 hrs of culture and virus infection was isolated and the generated libraries were sequenced by 50-bp single-end Illumina mRNA sequencing. Reads were aligned using Tophat v2.0.6 and bowtie v0.12.9; genomeCoverageBed was run on the resulting BAM files for the quantification of genomic coverage scaled using DESeq estimateSizeFactors. Exons and introns are indicated for each gene.

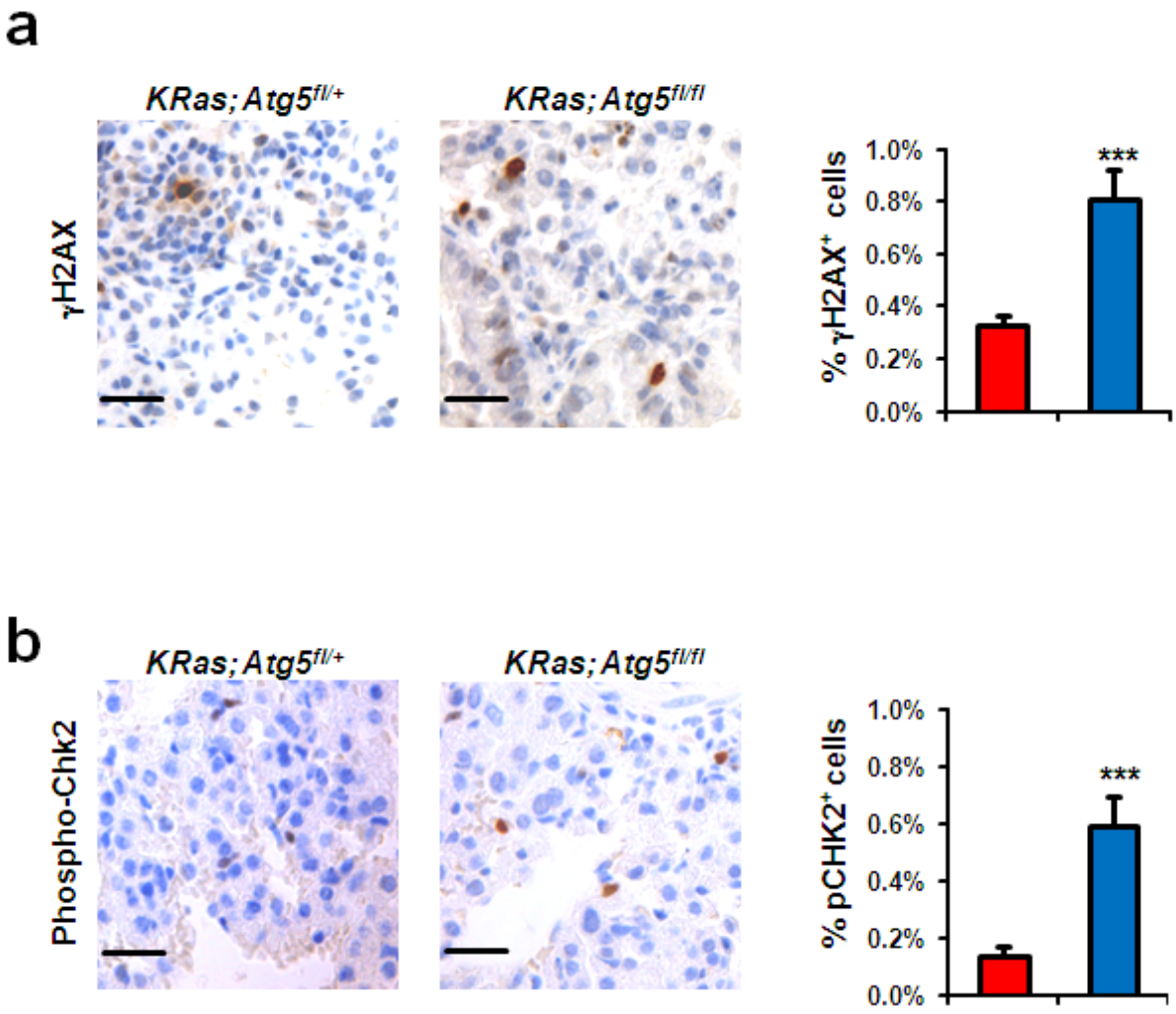


**Supplementary Figure 9. Activation of the DNA damage response in autophagy deficient lung tumors. (a,b)** Representative immunohistochemisty and quantitative assessment of **(a)** γH2AX and **(b)** phospho-Chk2 in lung tumors from *KRas;Atg5*$^{fl/+}$ and *KRas;Atg5*$^{fl/fl}$ littermates 6 wks after AdCre inhalation. At least 6 mice per genotype were analyzed. Quantifications are shown as mean percentages (± SEM) of positive cells per total cell numbers. Only cells within tumors were counted. Scale bars, 50μm. *** $P < 0.001$ (Chi-square tests of a generalised linear model with logit link assessing the genotype effect).

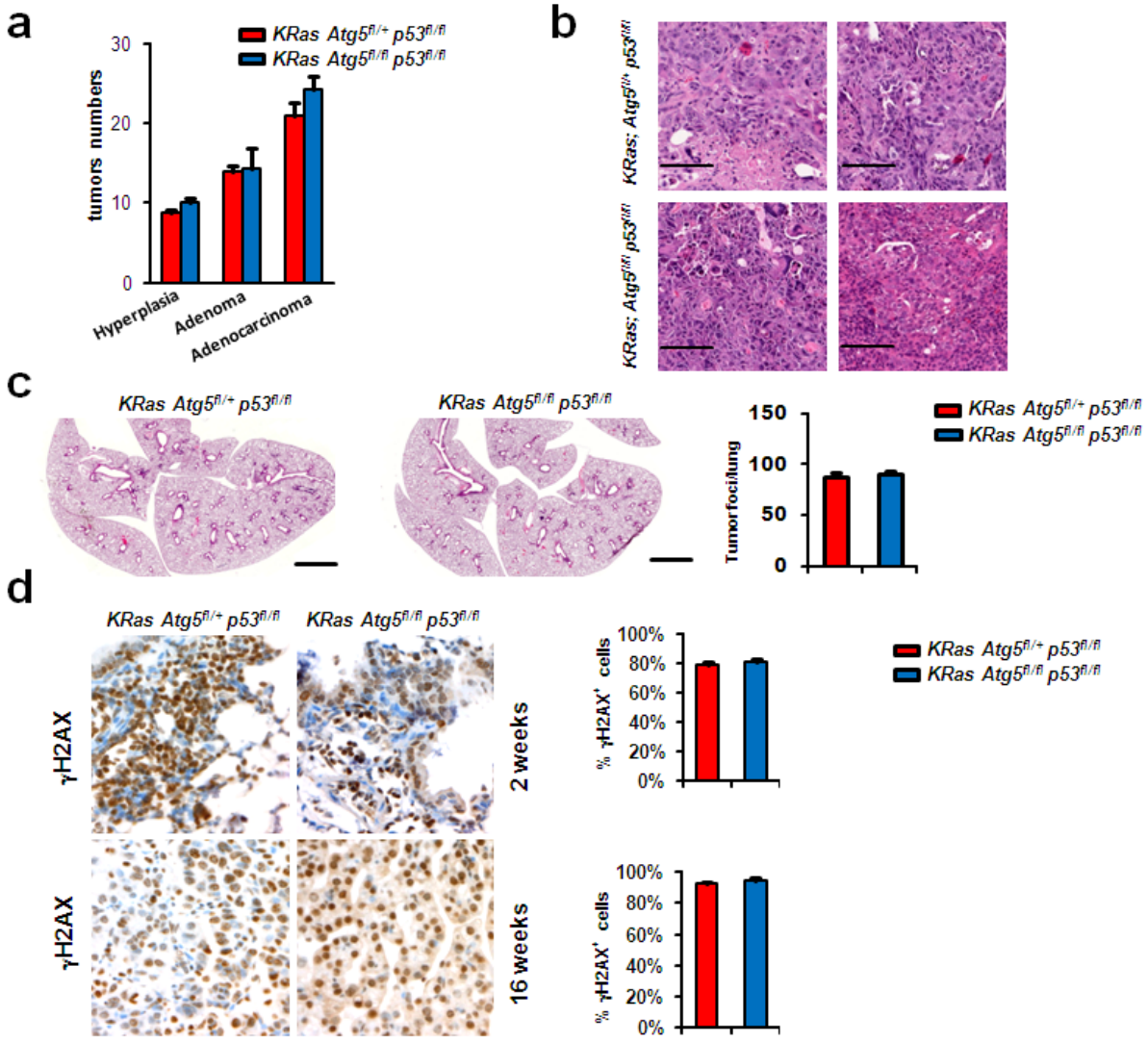


**Supplementary Figure 10. Loss of p53 in autophagy deficient KRas-driven lung tumors.** **(a)** Absolute numbers of hyperplastic lesions, adenomas, and adenocarcinomas in *KRas;Atg5*$^{fl/+}$*;p53*$^{fl/fl}$ and *KRas;Atg5*$^{fl/fl}$*;p53*$^{fl/fl}$ littermates 16 wks post-AdCre infection (n=4 per genotype). **(b)** Histological analyses of lung carcinomas in *KRas;Atg5*$^{fl/+}$*;p53*$^{fl/fl}$ and *KRas;Atg5*$^{fl/fl}$*;p53*$^{fl/fl}$ littermates 16 wks after AdCre inhalation. Representative H&E stainings are shown to demonstrate mitotic figures, irregular chromatin structures, and cellular and nuclear pleomorphism in lung tumors with the indicated genotypes. Size bars, 50µm. **(c)** Representative histological sections at 2 wks after AdCre inhalation are shown in the left panels. Scale bars, 2mm. Right panel shows quantification of numbers of hyperplastic lesions/per lung (mean values ± SEM) in *KRas;Atg5*$^{fl/+}$*;p53*$^{fl/fl}$ and *KRas;Atg5*$^{fl/fl}$*;p53*$^{fl/fl}$ littermates 2 wks after AdCre inhalation. n = 4 per group. **(d)** γH2AX in lung tumors from *KRas;Atg5*$^{fl/+}$*;p53*$^{fl/fl}$ and *KRas;Atg5*$^{fl/fl}$*;p53*$^{fl/fl}$ littermates 2 and 16 wks after AdCre inhalation. For γH2AX and phospho-Chk2 staining, sections were scored independently in a double-blinded fashion. Quantifications are shown as mean percentages (± SEM) of positive cells per total cell numbers. Only cells within tumors were counted. n=4 per group. Scale bars, 50µm.

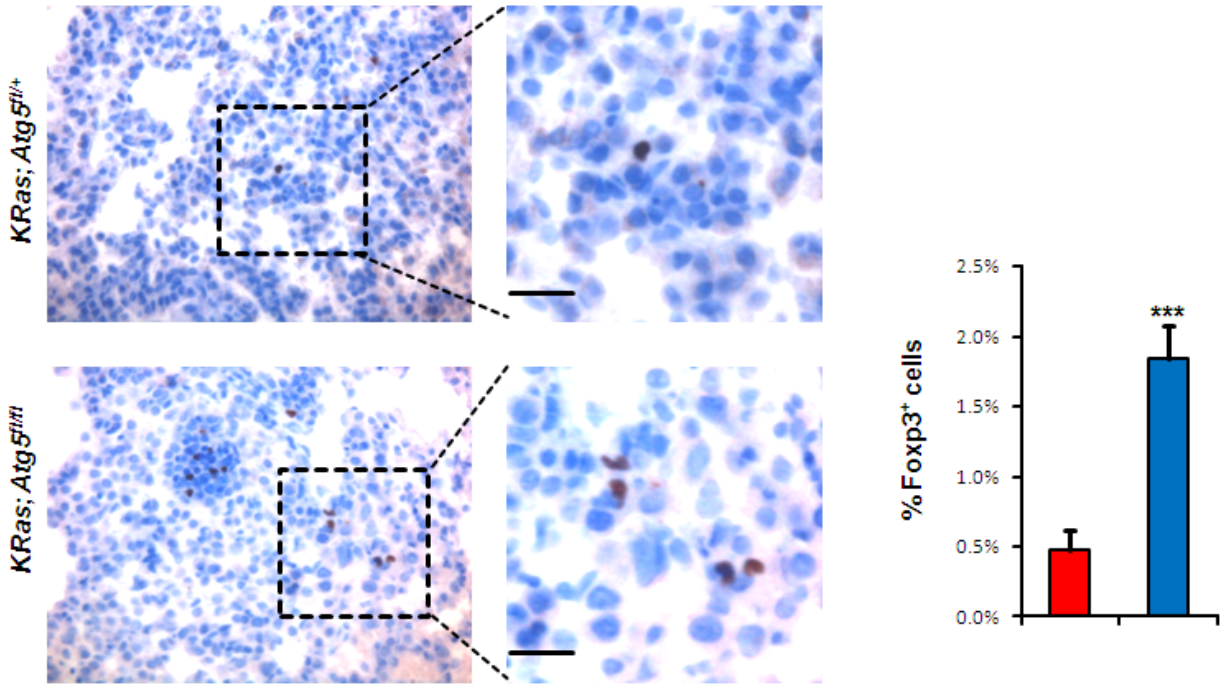


**Supplementary Figure 11. Treg accumulation in late lung tumors.** Representative immunohistochemisty and quantitative assessment of FoxP3$^{+}$ regulatory T cells in lung tumors from *KRas;Atg5*$^{fl/+}$ and *KRas;Atg5*$^{fl/fl}$ littermates 18 wks after AdCre inhalation. Data are shown as mean percentages (± SEM) of FoxP3$^{+}$ cells among total cell numbers in the tumor areas. Only cells within tumors were scored. At least 6 mice per genotype were analyzed. Size bars, 50 µm. *** P < 0.001 (Chi-square tests of a generalised linear model with logit link assessing the genotype effect).

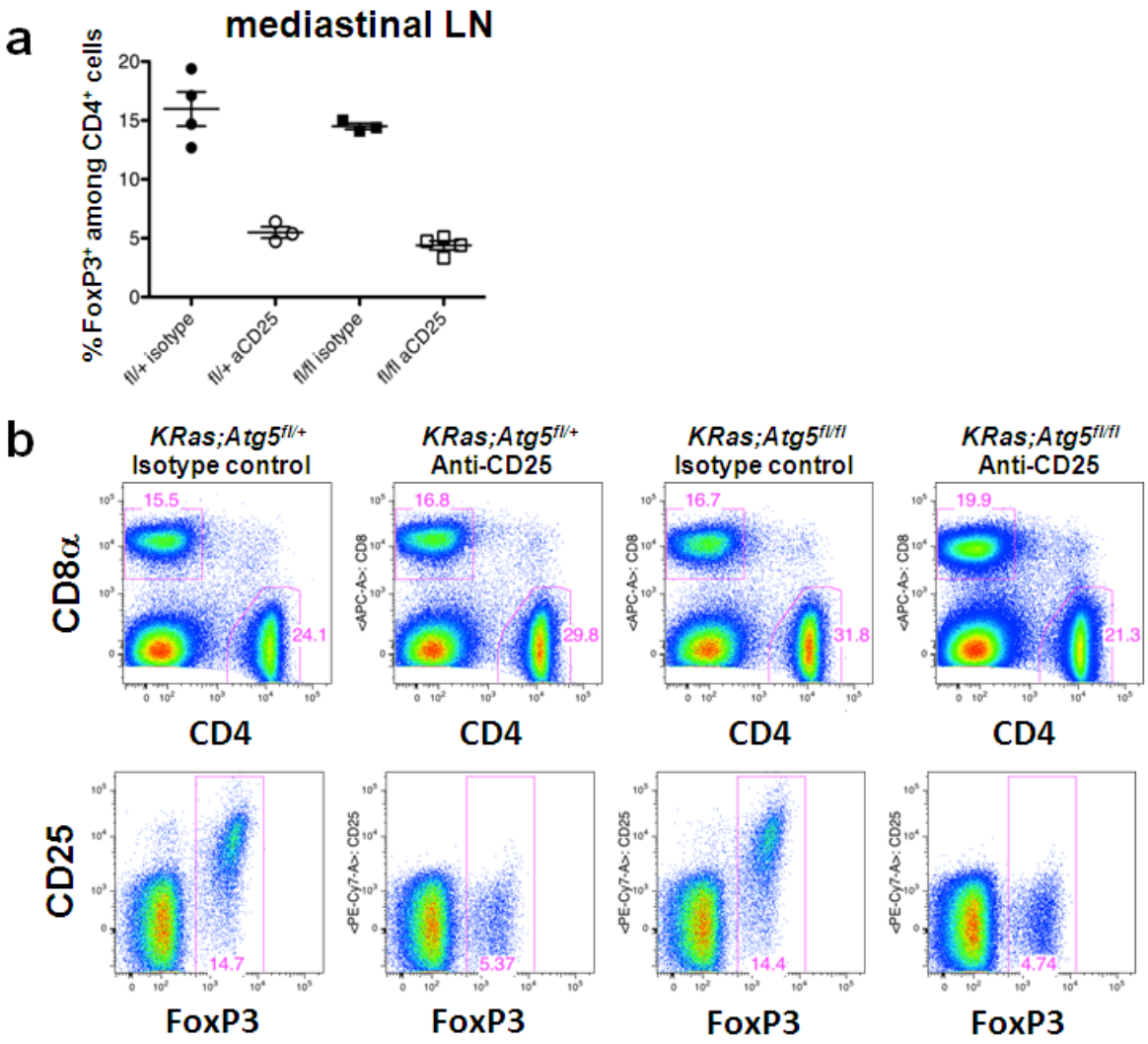


**Supplementary Figure 12. *In vivo* Treg cell depletion. (a)** FACS analyses to detect FoxP3$^+$ Treg and CD4$^+$ T cells in mediastinal lymph nodes from *KRas;Atg5$^{fl/+}$* (fl/+) and *KRas;Atg5$^{fl/fl}$* (fl/fl) littermates 2 wks after AdCre inhalation that either received control isotype antibodies (isotype) or depleting anti-CD25 Abs (αCD25). Cells were gated on CD4$^+$ populations and percentages of FoxP3$^+$ Tregs among CD4$^+$ T cells are shown for individual mice. Mean values (± SEM) are indicated. **(b)** Representative FACS analyses of lymphocytes incubated with antibodies specific for CD8α, CD4, CD25, and FoxP3. Cells were isolated from blood of *KRas;Atg5$^{fl/+}$* and *KRas;Atg5$^{fl/fl}$* littermates 2 wks after AdCre inhalation that either received control isotype antibodies or depleting anti-CD25 Abs. Numbers in dot blots indicate percentages of positive cells. Note the marked reduction in CD25$^+$FoxP3$^+$ Treg numbers after injection of αCD25, confirming the efficacy of the depletion protocol.

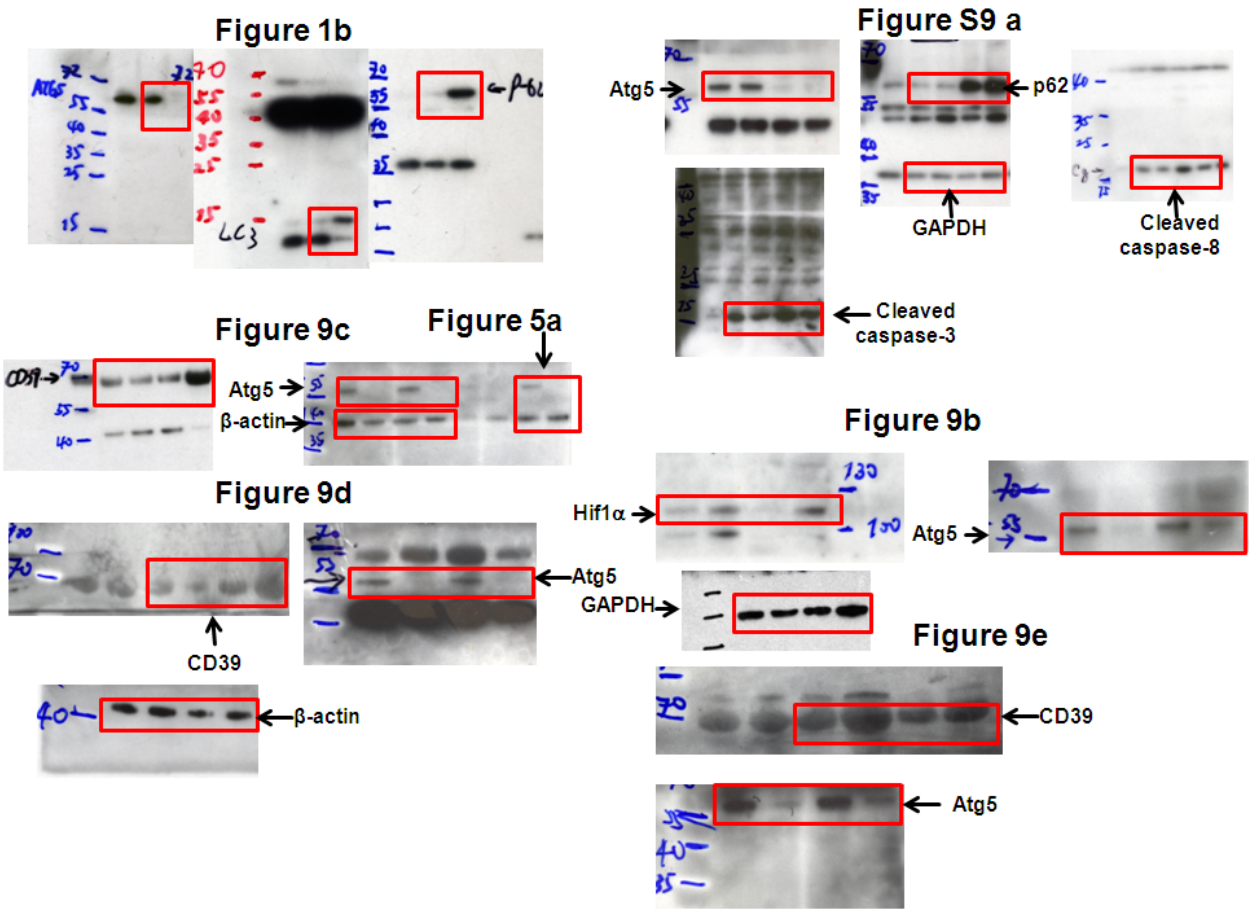


**Supplementary Figure 13. Images of the immunoblot results shown in the manuscript.** Red boxes indicate the cropped areas displayed in the indicated figures.